Available online at www.sciencedirect.com
ScienceDirect
Optics Communications 269 (2007) 14–23
OPTICS COMMUNICATIONS
www.elsevier.com/locate/optcom

Comprehensive modeling of the stationary and dynamic behaviour of imaginary Bragg gratings around threshold

Jacques M. Laniel [a], Mykola Kulishov [a,*], Nicolas Bélanger [a], José Azaña [b], David V. Plant [a]

[a] Department of Electrical and Computer Engineering, Photonic System Group, McGill University, Montreal, Que., Canada H3A 2A7
[b] Institut National de la Recherche Scientifique – Énergie, Matériaux et Télécommunications, 800 de la Gauchetière Ouest, suite 6900, Montreal, Que., Canada H5A 1K6

Received 9 March 2006; received in revised form 18 July 2006; accepted 25 July 2006

Abstract

This paper presents a dynamical study of an imaginary Bragg grating. It shows that when the lasing threshold is reached, the standard transmission matrix approach is no longer valid and a more comprehensive model taking in account gain saturation is required. The grating has then been studied using a direct numerical solution of the time-dependant coupled-mode equations including gain saturation effects. This description is valid for analyzing imaginary Bragg gratings operating both below and above the lasing threshold, and it has demonstrated to provide a physically consistent solution, avoiding the group delay divergences and abnormalities which are predicted by the transfer-matrix model.

1. Introduction

Periodic longitudinal perturbation of the complex dielectric permittivity composing an optical waveguide creates conditions for an effective co-directional and contra-directional guide mode interaction. When the periodicity is adjusted to achieve the phase-matching condition between a forward propagating mode and a backward one, the structure becomes a distributed feedback reflector or a Bragg grating.

In a Bragg grating, the reflected wavelength is determined by the grating periodicity while the coupling efficiency is determined by the transverse overlapping integral between the modulated dielectric permittivity and the propagating optical mode. The usual way to create a Bragg grating is to modulate the refractive index of the waveguide material either by periodically changing it through UV exposure or by periodically etching this material. This type of perturbation corresponds to a modulation of the real part of the dielectric permittivity (index Bragg grating). However, it is also possible to modulate the imaginary part of the dielectric permittivity. Such modulation creates a grating of alternating segments of gain and loss along the waveguide or a so-called *imaginary Bragg grating* (I-BG).

In their pioneer research, Kogelnik and Shank [1] analyzed distributed feedback (DFB) structures with periodic gain, i.e. I-BGs, in the small-signal (unsaturated) regime. They derived the lasing condition by solving the coupled-mode equations governing the coupling between the forward and backward propagating signals within the periodic structure. It was shown that a uniform I-BG has a single lasing mode exactly at the Bragg wavelength (for antireflection-coated facets). This interesting feature of a uniform I-BG was first suggested as a potential solution to the problem of spectral degeneracy of uniform index Bragg gratings in an amplifying guide, and was later confirmed experimentally by Nakano et al. [2].

Gain gratings have also attracted recent research interest for other various applications, including all-optical switching and routing and as tunable diffraction elements in laser systems [3–6]. It has been shown that these gratings exhibit

* Corresponding author. Present address: HTA Photomask Inc., San Jose, CA, USA. Tel.: +1 408 2599595.
E-mail addresses: mykola.kulishov@mcgill.ca, mykolak@htaphotomask.com (M. Kulishov).

0030-4018/$ - see front matter © 2006 Elsevier B.V. All rights reserved.
doi:10.1016/j.optcom.2006.07.055

many interesting features, including greater than unity diffraction efficiency and high spectral Bragg selectivity [6]. For example, a gain grating can be formed through spatial hole burning induced by the interference of two coherent beams inside a gain medium (e.g. laser amplifier) [4,5].

Other studies on the I-BGs have focused on the so-called gain-coupled distributed feedback (GC-DFB) lasers due to its higher single-mode yield and immunity to facet reflections [2]. Pure-gain-coupled lasers have been experimentally fabricated and tested, see for example [7]. In this context, two main approaches have been used to experimentally create an active gain/loss modulation [7,8]. In [7], the desired gain/loss periodic modulation was achieved by periodically etching an active layer. Then a second grating layer on top of the grating in the active layer was fabricated, thereby canceling out the effect of index coupling. The gain-coupled coefficients of this structure can be adjusted by controlling the strength of the injection current. A second approach to produce I-BGs is based on fabricating a periodic variation of loss along the waveguide [8]. The distinctive characteristic of such a structure is that the strength of the gain coupling is not affected by any change in the injection current.

It has been also demonstrated that an I-BG operating below its lasing threshold can be used as an optical filter, in which the filtered signal is additionally amplified [9–11]. Different designs of tunable optical filters based on I-BGs have been recently proposed [11]. It has been shown that wavelength tuning can be achieved by suitably adjusting the local gain-coupling and net gain in the structure.

In most of the previous works on I-BGs, these devices have been analyzed and designed using conventional coupled-mode theory. Important aspects in these structures such as the effects associated with gain saturation have not been considered. Notice that the effect of gain saturation is especially relevant when the I-BG operates near or above the lasing threshold. Moreover, most of the previous studies on I-BGs have been restricted to the CW regime and for instance, no detailed analysis of the dispersive properties of these devices has been provided. Obviously, the dispersion characteristics (and associated temporal, dynamic properties) of these devices are of fundamental importance when they are used for optical signal transmission and processing applications (e.g. when used as optical filters). In the authors' opinion, despite the past and increasing recent interest on I-BG-based configurations, there is a lack of detailed theoretical studies and numerical modeling of these devices.

The main motivation of this work is the development and testing of general and comprehensive models for the spectral-domain and temporal-domain analysis of I-BGs, including a detailed investigation on the range of validity of each one of the presented mathematical models. In our study, we consider a general gain/loss Bragg grating composed by periodically alternating segments of gain and loss. There are two regimes of interest for such gratings: below and above the lasing threshold. When the structure is below the threshold, we confirm that it can be accurately modeled and described using basic coupled-mode theory and the associated transfer matrix method. In this case, the device behaves as an amplifying optical filter. However, when the structure operates close or above the lasing threshold, the transfer matrix method is no longer valid. For instance, it is shown that the analysis of an optical I-BG filter using the transfer matrix method results in exotic numerical abnormalities in the grating's dispersion near the lasing threshold (e.g. superluminal group velocity). In order to properly describe the transmission characteristics of an I-BG above threshold, limiting mechanisms such as gain and loss saturation have been introduced in the mathematical model describing the reflector. In this case the problem can be solved using similar numerical procedure to that previously used by De Sterke et al. [12] for the analysis of the coupled-mode equations in the non-linear regime. In this way, we provide here a complete study of the dynamic (temporal) properties of the I-BGs over all the regimes of interest.

The remainder of this paper is organized as follows. Section 2 presents the theoretical background for the analysis of I-BGs, including its mathematical description in the form of a set of coupled-mode equations in combination with another set of equations to account for gain saturation effects. Two different methods are proposed and described for the solution of these equations, namely the conventional transfer-matrix approach (where no gain saturation effects are considered) and a more comprehensive model based on a direct numerical solution of the equations governing the I-BG behavior (including gain saturation effects). In Section 3 the range of validity of the conventional transfer-matrix technique is investigated and the method is applied to analyze the temporal impulse response of an I-BG below the lasing threshold. In Section 4, a direct numerical solution of the equations governing the I-BG is provided and applied to analyze the dynamic behavior of the I-BG (this includes the analysis of the stationary properties of the I-BG) both below and above the lasing threshold. Finally, in Section 5 we summarize and conclude our paper.

2. Theoretical modeling of imaginary Bragg gratings

2.1. Coupled mode equations

The study of the I-BG is based on the use of the coupled-mode theory formalism [1]. The gain and loss segments of the I-BG introduce a perturbation to the complex refractive index which allows the coupling between the forward and backward propagating modes. The perturbation is expressed as follows:

$$\Delta n(z) = \frac{\mathrm{j}}{k_0}\left[\Delta\alpha_{\mathrm{DC}} - \Delta\alpha_{\mathrm{AC}}\sin\left(\frac{2\pi}{\Lambda}z + \phi_{\mathrm{g}}\right)\right], \tag{1}$$

where $\Delta\alpha_{\mathrm{AC}}$ represents the loss/gain modulation amplitude, $\Delta\alpha_{\mathrm{DC}}$ is the average loss inside the grating (or gain if it is

negative), Λ is the grating period, $k_0 = 2\pi/\lambda$ with λ being the wavelength in vacuum, and ϕ_g accounts for a possible phase shift between the I-BG and the z-axis. Even though an imaginary contribution to the index of refraction also implies a change in the real part of the index of refraction through the Kramers–Kronig relations, we assume here that the real Bragg grating induced by the I-BG is negligible in comparison with the imaginary grating at its resonance wavelength. In practice, this approximation is valid if the gain material and its spectral dispersion properties are carefully selected [4].

The electric field of the propagating mode can be expressed as

$$E(z,t) = \frac{1}{2}[\widetilde{E}_+(z,t) + \widetilde{E}_-(z,t)]\mathrm{e}^{-\mathrm{j}\omega_0 t} + \text{c.c.}, \tag{2}$$

where ω_0 is the carrier angular frequency, $E(z,t)$ is the real electric field and $\widetilde{E}_\pm(z,t)$ represent the forward and backward complex electrical field of the propagating modes. The tilde on top of the character denotes that it is a complex quantity. The electric field can be further normalized in the following way:

$$\begin{aligned}\widetilde{E}_+(z,t) &= \widetilde{R}(z,t)\exp(\mathrm{j}\beta_g z),\\ \widetilde{E}_-(z,t) &= \widetilde{S}(z,t)\exp(-\mathrm{j}\beta_g z),\end{aligned} \tag{3}$$

where $\beta_g = \pi/\Lambda$ is the Bragg wavevector. Hence, considering a weakly guiding single-mode optical waveguide and no coupling allowed between the propagating modes and radiation modes, the coupled-mode equations take the following form [12]:

$$\begin{aligned}\mathrm{j}\left[\frac{\partial}{\partial z} + \frac{n_g}{c}\frac{\partial}{\partial t}\right]\widetilde{R} &= -\Delta\beta\widetilde{R} + \kappa\widetilde{S},\\ -\mathrm{j}\left[\frac{\partial}{\partial z} - \frac{n_g}{c}\frac{\partial}{\partial t}\right]\widetilde{S} &= -\Delta\beta\widetilde{S} - \kappa\widetilde{R},\end{aligned} \tag{4}$$

where κ is the coupling coefficient and $\Delta\beta(\omega) = \beta(\omega) - \beta_g$ is the mismatch factor. The coupling coefficient is determined by the transverse overlapping integral between the mode spatial profile and the AC contribution to the imaginary index introduced by Eq. (1) as $\Delta\alpha_{AC}$ [13]. The propagation constant can be defined with respect to the carrier frequency, ω_0, which fulfills the phase matching condition, as follows:

$$\beta(\omega) = \beta_g + \mathrm{j}\sigma + \frac{n_g}{c}(\omega - \omega_0), \tag{5}$$

where $\beta(\omega) = n(\omega)\omega/c$, $n(\omega)$ is the effective index of the propagating mode, n_g is the group index at the angular frequency ω_0, and σ is the average loss in the I-BG. A negative value of σ indicates an average gain instead of loss. For the sake of simplicity, the group index is assumed to be a real constant, which implies that the frequency dependence (and chromatic dispersion) of the average gain/loss is negligible.

As anticipated in the introduction, since the I-BG structure is able to sustain a lasing effect, it is important to include saturation mechanisms. The effect of gain saturation can be properly modeled by introducing an intensity dependence of the coupling coefficient and average gain/loss in the following way:

$$\kappa(z,I) = \kappa_{\text{loss}} + \frac{\kappa_{\text{gain}}}{1 + I(z,t)/I_{\text{sat}}}, \tag{6}$$

$$\sigma(z,t) = \sigma_{\text{loss}} + \frac{\sigma_{\text{gain}}}{1 + I(z,t)/I_{\text{sat}}}, \tag{7}$$

where κ_{loss} and σ_{loss} are respectively the loss contribution to the coupling coefficient and the average loss, κ_{gain} and σ_{gain} are respectively the non-saturated coupling coefficient and average loss due to the gain contribution. In this formalism, σ_{gain} is negative (see Eqs. (3) and (5)). Finally, I_{sat} is the saturation intensity and the intensity is given by

$$I(z,t) = |\widetilde{E}_+(z,t) + \widetilde{E}_-(z,t)|^2. \tag{8}$$

Eq. (4) can be solved using two different approaches. The first method, namely the conventional transfer-matrix formalism, is based on a stationary analysis of these equations, in which the saturation effects are not considered (Section 2.2). In this case, Eq. (4) can be solved analytically. The second method is based on a direct spatio-temporal numerical analysis of the same equations (Section 2.3), and allows one to include the saturation effects.

2.2. Basic transfer-matrix formalism

The first method implies a stationary solution, which means that the field amplitudes (complex envelopes) do not vary in time in Eq. (4). Furthermore, in this method, the saturation effects are neglected, i.e. $I/I_{\text{sat}} \ll 1$. Using these assumptions, Eq. (4) now becomes a standard scattering problem that can be solved analytically by using a transfer-matrix approach. The field amplitudes at the output of the grating (at $z = z_0 + L$) and at the input ($z = z_0$) are related in the following way:

$$\begin{bmatrix}\widetilde{E}_+(z_0+L)\\ \widetilde{E}_-(z_0+L)\end{bmatrix} = \begin{bmatrix}M_{11} & M_{12}\\ M_{21} & M_{22}\end{bmatrix}\begin{bmatrix}\widetilde{E}_+(z_0)\\ \widetilde{E}_-(z_0)\end{bmatrix}, \tag{9}$$

where z_0 is the position where the grating begins. The matrix elements are

$$\begin{aligned}M_{11} &= \left[\cos(\gamma L) + \mathrm{j}\frac{\Delta\beta}{\gamma}\sin(\gamma L)\right]\exp[\mathrm{j}\beta_g L],\\ M_{12} &= -\mathrm{j}\frac{\kappa}{\gamma}\sin(\gamma L)\exp[\mathrm{j}(\beta_g L + \phi_0)],\\ M_{21} &= -\mathrm{j}\frac{\kappa}{\gamma}\sin(\gamma L)\exp[-\mathrm{j}(\beta_g L + \phi_0)],\\ M_{22} &= \left[\cos(\gamma L) - \mathrm{j}\frac{\Delta\beta}{\gamma}\sin(\gamma L)\right]\exp[-\mathrm{j}\beta_g L],\end{aligned} \tag{10}$$

where $\gamma = (\kappa^2 + \Delta\beta^2)^{1/2}$ and $\phi_0 = 2\beta_g z_0 + \phi_g$. If a signal is injected at $z = z_0$ in the I-BG, the transmission and reflection characteristics of the I-BG can be obtained from Eqs. (9) and (10) assuming that no signal is injected at the grating output (i.e. $E_-(z_0 + L) = 0$),

$$r_+(z_0,L)=\frac{E_-(z_0)}{E_+(z_0)}=\mathrm{j}\frac{\kappa e^{-\mathrm{j}\phi_0}}{\gamma\cot(\gamma L)-\mathrm{j}\Delta\beta}, \tag{11}$$

$$t_+(z_0,L)=\frac{E_+(z_0+L)}{E_+(z_0)}=\frac{\gamma e^{\mathrm{j}\beta_g L}}{\gamma\cos(\gamma L)-\mathrm{j}\Delta\beta\sin(\gamma L)}, \tag{12}$$

where the "+" subscript indicates a forward propagation from $z=z_0$ to z_0+L. Both coefficients maximize their magnitudes at ω_0 as long as the imaginary part of the group index is negligible (as it has been assumed at Eq. (5)). In the case of a signal injected at $z=z_0+L$ and propagated backward towards $z=z_0$, the transmission and reflection coefficients are (the subscript "−" is used for the backward coefficients):

$$r_-(z_0,L)=-r_+(z_0,L)e^{2\mathrm{j}(\beta_g L+\phi_0)}, \tag{13}$$

$$t_+(z_0,L)=t_-(z_0,L). \tag{14}$$

The complex transmission and reflection coefficients given by Eqs. (11)–(14) provide a complete spectral description of the I-BG. The group delay and group velocity of the I-BG can be calculated from the grating complex transmission and reflection coefficients. The group delay will be an indication of the time spent by the propagating signal inside the grating. The group delay is defined from the phase of the reflection and transmission coefficients in Eqs. (11)–(14):

$$\left.\begin{matrix}\tau_r\\ \tau_t\end{matrix}\right\}=-\frac{\lambda^2}{2\pi c}\frac{\mathrm{d}}{\mathrm{d}\lambda}\left\{\begin{matrix}\arg(r),\\ \arg(t),\end{matrix}\right. \tag{15}$$

where the indices "±" have been dropped because Eqs. (13) and (14) show that the group delay in such uniform I-BG is independent of the direction of propagation through the I-BG. The group velocity is an indication of the speed at which the signal propagates along the grating. This quantity can only be defined in transmission and is given by the following relation:

$$v_g=\frac{L}{\tau_t}. \tag{16}$$

2.3. Direct numerical solution of the coupled-mode equations

The second method relies upon a direct numerical solution of the coupled-mode equations. The main advantage of this method is that it can include the nonlinear effects, namely gain/loss saturation effects. The gain/loss saturation is defined as in Eqs. (6) and (7) accordingly to the average intensity along one Bragg period Λ:

$$\begin{aligned}I_{\mathrm{avg}}(z,t)&=|\widetilde{E}_+(z,t)|^2+|\widetilde{E}_-(z,t)|^2\\&=|\widetilde{R}(z,t)|^2+|\widetilde{S}(z,t)|^2.\end{aligned} \tag{17}$$

It should be noted that the intensity saturation is not uniform inside one Bragg period due to the intensity oscillations induced by the interference between the forward and backward fields; however, the calculation of the gain saturation using the average intensity, as defined in Eq. (17), is an acceptable compromise that allows us to include the gain saturation effects into the numerical algorithm while avoiding the extreme complexity and computation costs associated with accounting for the intensity oscillations within the Bragg period. A possible consequence of this averaging would be to underestimate the saturation effect, leading to a greater signal. The precise effects of this approximation will be investigated in a subsequent publication where will be presented a theoretical model to evaluate the steady-state output power of an imaginary grating with saturation above the threshold.

To solve numerically the propagation equations presented by Eq. (4), we can use a similar approach to that developed by De Sterke et al. for solving the coupled mode equations in the nonlinear regime [12]. Specifically, a rescaling of the time variable and a rotation of the spatio-temporal frame of reference is first required. This was demonstrated to lead to a new set of differential equations which can be solved by a greatly simplified numerical algorithm [12]. Specifically, assuming the following change of variables:

$$\begin{aligned}T&=\frac{ct}{n_g},\\ z&=\zeta-\tau,\\ T&=\zeta+\tau,\end{aligned} \tag{18}$$

the coupled-mode equations becomes:

$$\begin{aligned}\mathrm{j}\frac{\partial\widetilde{R}}{\partial\zeta}&=-\Delta\beta\widetilde{R}+\kappa\widetilde{S},\\ -\mathrm{j}\frac{\partial\widetilde{S}}{\partial\tau}&=-\Delta\beta\widetilde{S}-\kappa\widetilde{R}.\end{aligned} \tag{19}$$

The details of the numerical method to solve the Eq. (19) will not be reviewed here because they are beyond the scope of the present paper. The reader is referred to the work by De Sterke's et al. for a detailed description on this numerical method [12]. It should be noted that Eq. (19) are exactly the same as the ones derived in [12] except for the inclusion of nonlinear saturation effects. Since these effects (shown in Eqs. (6) and (7)) depend only on the field and the spatial and temporal coordinates, they can be easily included in De Sterke's et al. method. In fact, the explicit presence of z and t in the right hand-side of Eq. (4) would have not allowed the essential change of variables described by Eq. (18).

3. Transfer-matrix method: application and validity

3.1. Analysis of lasing threshold

The presence of gain within the I-BG allows the structure to undergo lasing effect. In particular, the I-BG structure presents a threshold above which a lasing effect will occur inside the grating; in this case, the grating acts as a distributed Bragg reflector (DBR) laser.

The threshold condition can be found by use of the analytical solution obtained for the I-BG via the

transfer-matrix method [1]. The lasing condition in the I-BG dictates that the matrix element M_{22} should be equal to zero. This condition coincides with the poles of the transmission and reflection coefficients and represents the fact that when the I-BG is lasing, there may be outgoing signals even with no inputs. Assuming a homogenous gain, only the angular frequency ω_0 experiencing the highest gain through the I-BG can reach the lasing threshold. This leads to the lasing threshold condition expressed as [1]

$$\kappa L = \begin{cases} \cosh^{-1}(-\sigma/\kappa)/\sqrt{(\sigma/\kappa)^2 - 1} & \text{for } \sigma \leqslant -\kappa, \\ \cos^{-1}(-\sigma/\kappa)/\sqrt{1 - (\sigma/\kappa)^2} & \text{for } -\kappa \leqslant \sigma < \kappa, \end{cases} \tag{20}$$

where σ is the DC loss (or gain, if negative) introduced in Eq. (5). Two particular cases have to be pointed out. Firstly, the singularity at $\sigma = -\kappa$ can be solved to find that for such a case, $\kappa L = 1$. Secondly, in this paper, we focus on the case with no DC gain/loss in the I-BG, i.e. $\sigma = 0$; in this case, the lasing condition in Eq. (20) occurs exactly for $\kappa L = \pi/2$.

In our study, we have found an interesting inconsistency when evaluating the grating group delay around the lasing threshold using the conventional transfer-matrix method. Fig. 1 shows the transmission and reflection properties for two distinct grating strengths at both sides of the threshold condition, $\kappa L = 0.45\pi$ and 0.55π. The grating period is $\Lambda = 0.5$ μm, its length is $L = 15$ μm and the effective index is $n_{\text{eff}} = 1.55$. The Bragg wavelength for such a grating is 1.55 μm. For the sake of simplicity, dispersion of the mode's effective index is neglected.

Fig. 1 shows several interesting characteristics. The group delay obtained for the two grating strengths are quite different from one another. In Fig. 1(c), one can observe an abnormal discontinuity in the group delay curve around the Bragg wavelength, which undergoes a complete reversal from a large positive value (solid curve) to a large negative value (dashed curve) when crossing the threshold point at $\kappa L = 0.5\pi$. Besides this abnormal group-delay "discontinuity" (around the lasing threshold), the negative group delay above threshold seems to indicate a superluminal propagation effect, meaning that the signal gets out of the I-BG even before entering it. We anticipate that these paradoxical results are associated with the mathematical model rather than any real physical phenomenon. The stationary model is not valid above and even close to the lasing threshold. A further indication of the lack of validity of the basic transfer-matrix model around and above threshold conditions is that in the case of operation at the exact lasing threshold, i.e. for $\kappa L = 0.5\pi$, the transmission and reflection spectra calculated via the transfer-matrix method strongly diverge (at the Bragg wavelength) and exhibit a spectral width close to zero.

We have developed a testing strategy for the transfer matrix model based on comparing the results from two different approaches, both based on this same model. In the first one the model is applied to the whole I-BG structure which can be above the threshold condition ($\kappa L > 0.5\pi$), while in the second approach, we analyze the result of considering a concatenation of two shorter I-BGs, each of them operating below the threshold condition ($\kappa(L - \delta z) < 0.5\pi$; $\kappa\delta z < 0.5\pi$). The expressions of reflection and transmission spectral coefficients through the I-BG according to the basic transfer-matrix model are given by Eqs. (11) and (12). Fig. 2 presents the alternate way of calculating

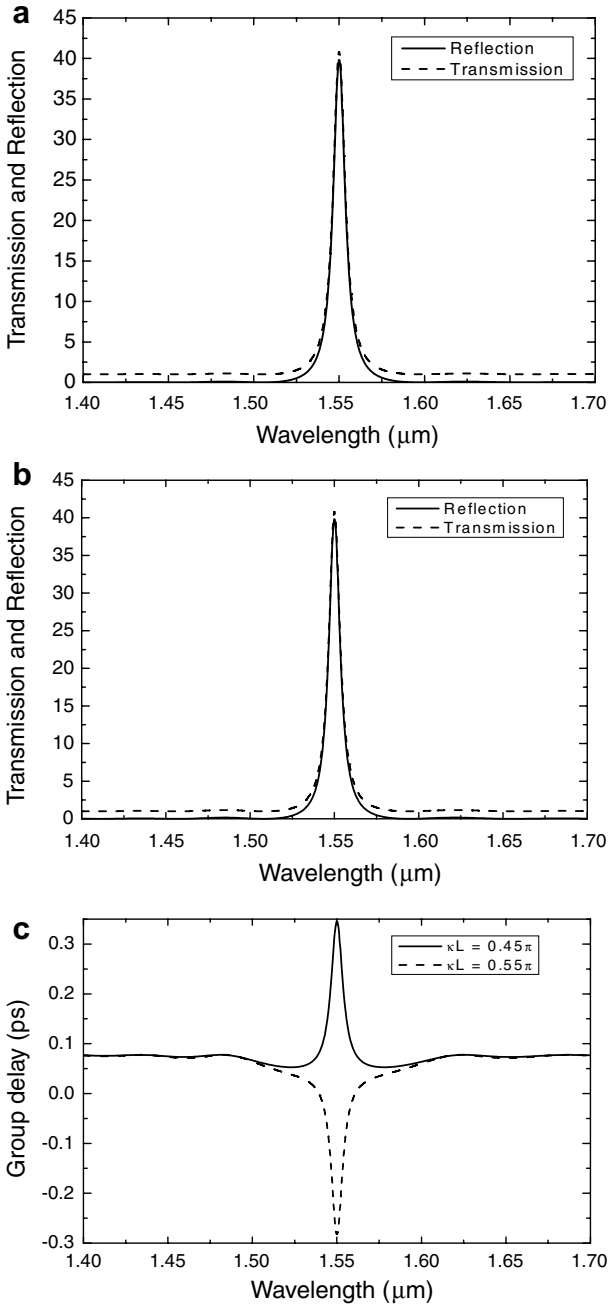

Fig. 1. Transmission and reflection characteristics of the I-BG below and above the lasing threshold with $\sigma = 0$. The transmission and reflection spectra are shown for $\kappa L = 0.45\pi$ (below threshold) in (a) and 0.55π (above threshold) in (b). The group delays in transmission for both grating strengths are shown in (c).

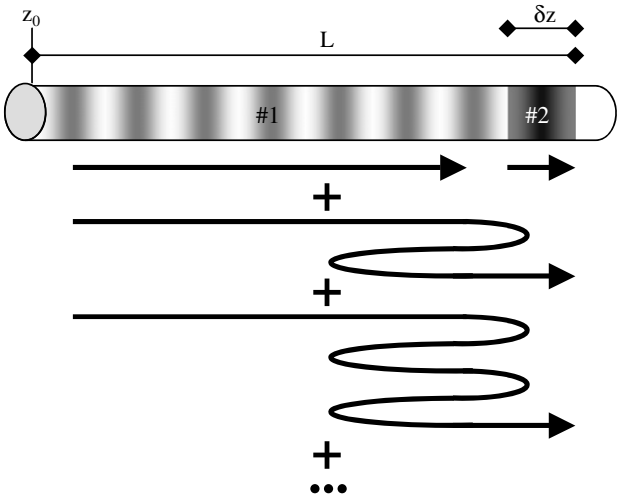

Fig. 2. Modeling the I-BG as composed by the concatenation of two imaginary sub-gratings.

the transmission of the same I-BG as a sum of signals bouncing back and forth between the two concatenated gratings. The first grating labeled as #1 starts at z_0 and has a length of $L-\delta z$, while the second one labeled as #2 starts at $z_0+L-\delta z$ and has a length of δz. The overall grating starts at z_0 and has a length of L. Using the grating concatenation modeling, the transmission coefficient through the whole structure can be calculated as:

$$t_{\mathrm{tot}+}=t_{1+}t_{2+}\sum_{n=0}^{\infty}(r_{2+}r_{1-})^n, \tag{21}$$

where the indices 1 and 2 refer to each sub-grating. Using the same procedure, a similar expression can also be obtained for the reflection coefficient:

$$r_{\mathrm{tot}+}=r_{1+}+t_{1+}r_{2+}t_{1-}\sum_{n=0}^{\infty}(r_{2+}r_{1-})^n. \tag{22}$$

The same geometric series appears in the last two equations, and this geometric series converges to $1/(1-r_{2+}r_{1-})$ as long as κL is kept under the lasing threshold presented at Eq. (20) because the condition in Eq. (20) ensures that $|r_{2+}r_{1-}|<1$. Moreover, it is only when the infinite sum converges that Eqs. (21) and (22) simplify to the previous transmission and reflection coefficients obtained via the transfer-matrix method, i.e. expressions in Eqs. (12) and (11). The fact that the series in Eqs. (21) and (22) do not converge above the lasing threshold confirms the anticipated inconsistency of the basic transfer-matrix model in this case. The origin of the discrepancies observed above the lasing threshold can be addressed more rigorously by evaluating the temporal impulse response of the I-BG.

3.2. Temporal impulse response of the I-BGs

The concatenation of two gratings implies an infinite sum of terms, each one delayed in respect to the previous one by the round trip time between these two gratings. Based on this, one would expect that a truncated sum, only including a few terms of the whole series, could still provide an accurate estimate of the grating response for sufficiently small times. Thus, a comparison between the grating time responses provided by the transfer-matrix method and the concatenation of two grating should provide a deeper insight into the method's validity and origin of the observed discrepancies above the lasing threshold.

The temporal impulse response of both the sub-gratings structure and the whole grating structure can be obtained by a numerical inverse Fourier transform of the corresponding grating spectral response. In Fig. 3, the temporal impulse response of the I-BG in transmission obtained from the transfer matrix method (inverse Fourier transform of Eq. (12)) is compared with that obtained by considering the concatenation of two identical gratings of length $L/2$ (inverse Fourier transform of Eq. (21)). The comparison is carried out for both cases below the lasing threshold, Fig. 3(a), and above the threshold, Fig. 3(b).

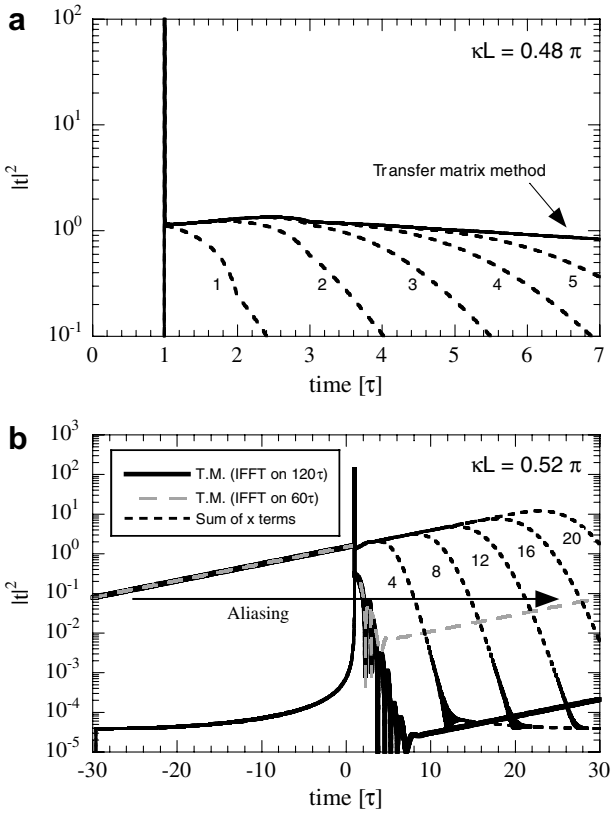

Fig. 3. Intensity of the temporal impulse response in transmission for the I-BG with no DC loss ($\sigma=0$) (a) below the lasing threshold with $\kappa L=0.48\pi$, and (b) above the lasing threshold with $\kappa L=0.52\pi$. The dotted lines are the results obtained assuming the concatenation of two gratings of length $L/2$, as given by Eq. (21). The number on each dotted line indicates the number of terms included for the calculation of this curve. The Inverse Fast Fourier Transform (IFFT) of the spectral response of the whole I-BG using the transfer matrix method is also presented for two different widths of the temporal window used for the IFFT calculation: 120τ for the solid black line, and 60τ for the dashed grey line.

The origin of time (zero) corresponds to the moment of impulse injection into the I-BG and the time axis is in the units of the time propagation τ through the unperturbed waveguide of length L (assuming there is no I-BG in the waveguide), $t' = t/\tau$.

Fig. 3(a) shows that below the lasing threshold, the temporal impulse response obtained by direct application of the transfer-matrix method is reconstructed by summing up a sufficiently large number of terms in the infinite sum (series) resulting from the application of the two concatenated half-gratings model. This is consistent with our previous results in Section 2.2, confirming the validity of the basic transfer-matrix method for obtaining the I-BG response in both the spectral and temporal domains. In particular, Fig. 3(a) shows that the temporal impulse response of the I-BG below threshold exhibits a Dirac delta-function at the time τ, i.e. propagation time along the unperturbed waveguide of length L (waveguide without grating). This time delta-function is followed by a slowly decreasing tail, as predicted by the transfer-matrix method and as reconstructed by the two concatenated gratings model. As expected, a larger number of terms in the series are required for an accurate reconstruction at longer times.

Above the lasing threshold, there is a significant discrepancy between the two methods. Fig. 3(b) shows that the transfer matrix method now predicts a decreasing tail in the impulse response toward negative times. The use of two different temporal windows for the inverse Fourier transform shows that the tail in the right side is just a numerical artifact due to the aliasing of the tail in the left side. The average temporal position of such an impulse response, also called group delay, now becomes smaller than τ, which is consistent with our previous predictions of a superluminal propagation effect above threshold (in some cases, with a pulse coming out from the I-BG even before it has been injected at the input). On the other hand, the concatenation of the two half-gratings rather gives an increasing tail toward positive times, with no energy before $t = \tau$.

It should be noted that from a mathematical point of view, the observed impulse response, diverging to infinity as the time increases, does not have an inverse Fourier transform [14]. This result indicates that a grating above the lasing threshold cannot be described through its transfer function in the spectral domain, i.e. through the conventional reflection and transmission coefficients obtained from the transfer-matrix method in Eq. (11). Physically, it means that the input signal undergoes a net gain at each round trip inside the I-BG. This net gain increases the output power until it is stabilized by the effect of gain saturation. Thus, as anticipated above, the main reason why the basic transfer-matrix model cannot be applied above lasing threshold is that this model does not consider gain saturation effects. To fully and accurately analyze the behavior of an I-BG, a direct numerical solution of the coupled-mode equations, including gain saturation effects, is required.

As soon as we get over the threshold condition, $\kappa L > \pi/2$, the transfer matrix method gives the finite solution for the transmission at the resonance wavelength until we again achieve the next threshold condition. This solution given by the transfer matrix method implies the presence of a signal inside the I-BG before any pulse is injected. This small light signal slowly increases its intensity from the amplification provided by the I-BG. In order to prevent divergence in the solution, this small signal has the proper intensity and phase to destructively interfere with the pulse when it is injected. Therefore, no light is left inside the I-BG after the injection of the pulse: all the power inside the I-BG has been extracted at the moment the pulse is injected. The only light emitted by the I-BG was produced by the light initially present in the grating before the injection of the pulse. This explains why the transfer matrix method seems to lead to super-luminal propagation.

4. Comprehensive modeling and analysis of the I-BGs

In order to better ascertain the actual behavior of the I-BG, it is necessary (i) to include gain saturation effects in the grating model and (ii) to evaluate the transmission and reflection of pulses directly in the temporal domain, instead of restricting the analysis to CW signals (spectral domain analysis). This can be achieved by solving Eq. (4) with the coupling coefficient defined by Eq. (6) and the DC loss defined by Eq. (7). As discussed in Section 2.3, the method that we have used to solve these equations is purely numerical and is based on the formalism developed by De Sterke et al. [12] to deal with the problem of non-linear propagation in a waveguide/fiber Bragg structure.

The DC contributions of loss and gain are set to cancel each other when the grating is unsaturated, i.e. $\sigma(z,0) = \sigma_{\text{loss}} + \sigma_{\text{gain}} = 0$. However, they cannot be equal to zero. In fact, a grating of loss would have regions of gain if its DC component is not large enough compared to its AC components, which does not make any sense. The inverse argument applies for the gain grating. For instance, assuming purely sine-shaped loss and gain gratings, this condition implies that $\sigma_{\text{loss}} \geqslant |\kappa_{\text{loss}}|$ and $\sigma_{\text{gain}} \leqslant -|\kappa_{\text{gain}}|$. Finally, for simplicity, the gain saturation is assumed here to be instantaneous which prevent from observing undershoot when a signal is injected and overshoot after passing through the I-BG.

4.1. Dynamical analysis of an I-BG below the lasing threshold

The first considered case is when the grating strength is below the lasing threshold. The dynamics of the I-BG below threshold ($\kappa L < 0.5\pi$ with $\sigma(0) = 0$) is analyzed by injecting a Gaussian pulse inside the structure. The boundary conditions now become:

$$\widetilde{R}(0,t) = A_0 \exp\left[-\frac{(t-t_c)^2}{2t_0^2}\right], \qquad \widetilde{S}(L,t) = 0, \tag{23}$$

where A_0 is the Gaussian amplitude, t_c is the center time of the input Gaussian pulse and t_0 is the input pulse duration. Fig. 4 shows the injected, reflected and transmitted signals through the I-BG with the same grating specifications as those used in Fig. 1. The center time is $t_c = 5.04$ ps, and the pulse duration is $t_0 = 0.25$ ps, which corresponds to a bandwidth of 10.2 nm (this bandwidth is of the same order as the grating bandwidth of ~8.8 nm). The saturation effect is taken into account in these simulations and in particular, it is adjusted so that $I_{max}/I_{sat} = 1.0$, the DC loss is zero and the grating strength is $\kappa L = 0.45\pi$, which is under the lasing threshold. As expected, the transmitted and reflected pulses are delayed and slightly distorted (broadened) as compared with the input pulse. The transmitted signal is also amplified with respect to the injected one. The gain is provided by the imaginary grating and is limited by the saturation effect. The reflected beam is less amplified since it does not penetrate deep into the I-BG.

It should be noted that the results shown in Fig. 4 are consistent with those expected from the group delay and group velocity curves predicted by the transfer-matrix model. In fact, similar results to those shown in Fig. 4 could have been obtained by use of the transfer-matrix method (by simply convolving the input Gaussian pulse with the temporal impulse response of the grating obtained in the previous section). We reiterate however that the method used here also takes into account the gain saturation effect, which is obviated in the transfer-matrix method – the direct numerical analysis used here provides thus a somehow more complete and accurate picture of the grating behavior even below the lasing threshold. Moreover, the information directly provided by the transfer-matrix method (behavior in the CW region for different frequencies or in other words, grating spectral behavior) can be also obtained from the direct numerical method by using a CW signal (pure sinusoids) as the input waveform (instead of a Gaussian pulse, as in the example shown here). We have conducted these calculations and have obtained the same transmission and reflection spectra, group velocity and group delay curves as those obtained by the transfer-matrix method and shown in Fig. 1(a)–(c).

4.2. Dynamical analysis of the I-BG above the lasing threshold

The second case considered is when the grating strength is equal or greater than the lasing threshold ($\kappa L \geqslant 0.5\pi$ with $\sigma(0) = 0$). Assuming a Gaussian pulse with a temporal duration t_0 of 0.25 ps, injected in the I-BG that is already lasing a CW signal corresponding to its steady-state, the transmitted and reflected signals have been numerically evaluated for two cases: first, the case where the grating strength is varied from $\kappa L = 0.5\pi$ to 1.0π for a fixed ratio $I_{in,max}/I_{sat} = 1.0$; and the second case where $I_{in,max}$ is kept at 1.0 and I_{sat} is varied from 0.1 to 0.8 for a fixed grating strength of $\kappa L = 0.7\pi$. In both cases we assume a center time of $t_{in} = 5$ ps for the input Gaussian pulse. Figs. 5 and 6 show the transmitted and injected signals for the two analyzed cases.

Figs. 5 and 6 give a complete picture of the I-BG dynamics when the grating is operated above the lasing threshold. In all the cases, the causality principle is respected, since the peak of the outgoing signal is delayed with respect to the peak of the injected signal. However in all cases, except at the exact threshold point, our results show the presence of a CW component in the cavity. This is evidenced by the continuous background in the simulated temporal responses; this behavior is expected since for $\kappa L \geqslant 0.5\pi$, the cavity can undergo lasing. In particular, Fig. 5 shows that the CW intensity (background in the temporal responses) is proportional to the grating strength and is therefore proportional to the gain present in the structure. In the case of $\kappa L = 0.5\pi$ (exact threshold point) there is no CW signal. Fig. 6 shows that the CW signal increases

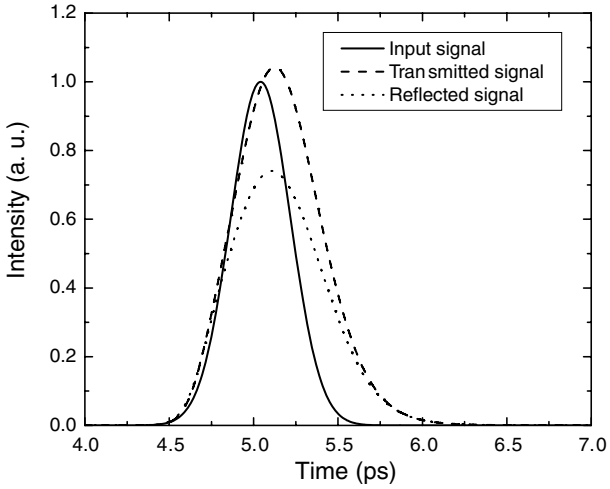

Fig. 4. Injected, transmitted and reflected signal through the I-BG with no DC loss, assuming a Gaussian input pulse. Gain saturation effect are included, $I/I_{sat} = 1.0$. The grating strength is $\kappa L = 0.45\pi$.

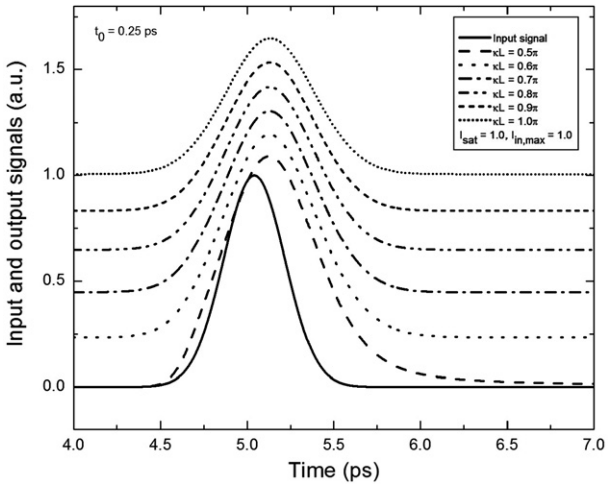

Fig. 5. Temporal shape of the incident and transmitted pulses for an injected signal of $t_0 = 0.25$ ps and grating strengths varying from $\kappa_0 L = 0.5\pi$ to 1.0π.

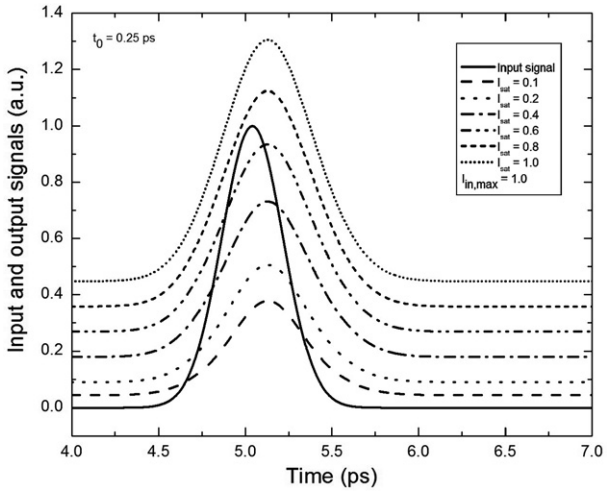

Fig. 6. Temporal shape of the incident and transmitted pulses for a grating strength of $\kappa L = 0.7\pi$ and $t_0 = 0.25$ ps with varying saturation intensities from $I_{sat} = 0.10$, 0.20, 0.40, 0.60 and 0.80. The maximum intensity of the injected signal is always 1.00.

for a greater saturation intensity (i.e. for less saturation). Thus, as expected, the grating strength and the saturation intensity are the main factors that determine the magnitude of the CW amplitude.

4.3. Group delay above and below threshold

It is interesting to examine closer the group delay between the pulse injected in the I-BG and the one transmitted as a function of the grating strength. Even though the notion of group delay cannot be formally defined for nonlinear propagation (which is the case in the presence of saturation effect), an "average" group delay can be estimated by measuring the time between the peaks of the input and output pulses. Fig. 7 shows the group delay computed as a function of the grating strength κL for different saturation intensities. The grating and pulse characteristics are exactly the same as those assumed in Sections 4.1 and 4.2. One can see that for the case of no saturation, which correspond to $I_{sat} \to \infty$, the group delay above threshold is anomalous. This is caused by the fact that this group delay have been obtained with the matrix approach which is not valid above the threshold. The abrupt shift around the threshold point from a high group delay to a very small one is exactly the same as that shown in Fig. 1(c). This non-physical behavior in the group delay function does not present in the simulation results because the saturation is included. One can see that in all cases when the saturation is finite, the group delay behavior around and above the threshold is continuous and is not negative anymore for $\kappa L > \pi/2$. However, when the saturation becomes negligible (high value of I_{sat}), the group delay below threshold tend toward the group delay with no saturation, as expected. Fig. 7 shows once more that the inclusion of saturation effects removes efficiently the divergence in the solution of the propagating signal inside the I-BG. It is also interesting to point out that at $\kappa L = \pi$ the group delay at high saturation level converges toward zero which coincides with the result of the transfer matrix method. This superluminal behavior of the I-BG remains to be studied.

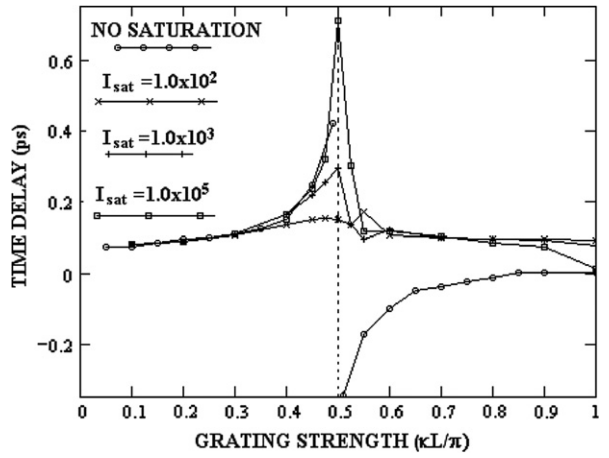

Fig. 7. Group delay between the injected pulse and the transmitted one as a function of the grating strength κL. The maximum intensity of the injected pulse was kept at $I_{in,max} = 1$ while the saturation intensity was varied from 1.0×10^2 to 1.0×10^5. Solid curve with circles represents the result of transfer matrix simulation without saturation effect.

5. Conclusion

In this paper, the dynamic behavior of the I-BG has been analyzed for two different cases: when the structure is operated below and above the lasing threshold. First, the I-BG has been modeled using the conventional transfer-matrix approach for solving the associated coupled-mode equations. Such an approach was demonstrated to be a valid one to derive the lasing threshold conditions and describe the I-BG below the threshold. A fundamental limitation of the transfer-matrix method is that the gain saturation effects are not accounted for in the I-BG model. As a result, when the threshold is reached and exceeded, this approach provides diverging solutions and predicts a superluminal propagation effect. These results violate the basic principle of causality and in fact, we have concluded that the transfer-matrix approach is not a valid method to study the I-BGs near the threshold and above it. The non-physical diverging response of the I-BG obtained above the lasing threshold has also suggested the need for including a saturation mechanism similar to that conventionally used in laser theory.

The I-BG has then been studied using a direct numerical solution of the time-dependant coupled-mode equations including gain saturation effects. This numerical problem has been solved using a similar approach to that reported by De Sterke et al. for the analysis of non-linear Bragg couplers [12]. The inclusion of gain saturation into the dynamical I-BG equations has been demonstrated to provide a more complete and more accurate description of the I-BG. This description is valid for the I-BG operation below and above the lasing threshold, providing a solution without

the group-delay divergences and abnormalities predicted by the transfer-matrix model. The direct numerical solution of the I-BG problem was applied to the study of the dynamic behavior of an I-BG (analysis of short pulse propagation through the I-BG) below and above the threshold. We believe that the availability of a comprehensive model of I-BGs with a tested wide range of validity should prove very useful for applications requiring a deep understanding of the spectral and temporal properties of these devices.

Acknowledgements

This work was supported by the Natural Sciences and Engineering Research Council (NSERC) and industrial and government partners, through the Agile All-Photonic Networks (AAPN) Research Network.

References

[1] H. Kogelnik, C.V. Shank, J. Appl. Phys. 43 (1972) 2327.
[2] Y. Nakano, Y. Luo, K. Tada, Appl. Phys. Lett. 55 (1989) 1606.
[3] M.J. Damzen, R.P.M. Green, K.S. Syed, Opt. Lett. 23 (1995) 1093.
[4] Y.O. Barmenkov, A.V. Kir'yanov, M.V. Andres, IEEE J. Quantum Electron. 41 (2005) 1176.
[5] A.W. Brown, M. Xiao, Opt. Lett. 30 (2005) 699.
[6] R.P.M. Green, G.J. Crofts, M.J. Damzen, Opt. Commun. 102 (1993) 208.
[7] Y. Luo, Y. Nakano, K. Tada, T. Inoue, H. Hosomatsu, H. Iwaoka, Appl. Phys. Lett. 56 (1990) 1620.
[8] H.-L. Cao, Y. Nakano, K.Tada, Y.Luo, M.Dobashi, H.Hosomatsu, Low threshold and high-mode yield MQW gain coupled DFB laser, Tech. Dig. 4th Optoelectron. Conf. (OEC'92) Makuhari Messe, Japan, paper PD-3, July 1992, p. 6.
[9] K. Magari, H. Kawaguochi, K. Oe, M. Fukuda, IEEE J. Quantum Electron. 24 (1988) 2178.
[10] J. Willems, K. David, G. Morthier, R. Baets, Electron. Lett. 27 (10) (1991) 831.
[11] K.Y. Lim, A.L.Y. Low, S.F. Chien, H. Ghafouri-Shiraz, IEEE J. Select. Topics Quantum Electron. 11 (5) (2005) 913.
[12] C.M. de Sterke, K.R. Jackson, B.D. Robert, J. Opt. Soc. Am. B 8 (1991) 403.
[13] D. Marcuse, Theory of Dielectric Optical Waveguides, second ed., Academic Press, Boston, San Diego, New York, 1974.
[14] A. Papoulis, The Fourier Integral and its Applications, McGraw-Hill, New York, 1987.